

Loss of nucleobindin-2 causes nigrastriatal degeneration in mice by impacting circadian rhythm-related genes and gut microbiota

Shengnan Liu

Qingdao University

Ruihan Song

Center for Maternal and Child Care and Birth Control of Qingdao

Ruofan Wu

Qingdao University

Xiao Kong

Qingdao University

Xiaoli Shen

shenxiaoli@qdu.edu.cn

Qingdao University

Article

Keywords: Nucb2, Nesfatin-1, Parkinson's disease, dopaminergic neurons, circadian rhythm, gut microbiota

Posted Date: August 27th, 2025

DOI: https://doi.org/10.21203/rs.3.rs-7332954/v1

License: © ① This work is licensed under a Creative Commons Attribution 4.0 International License.

Read Full License

Additional Declarations: No competing interests reported.

Abstract

Nesfatin-1 is a brain-gut peptide encoded by the nucleobindin-2 (NUCB2) gene. We previously demonstrated that a reduced level of nesfatin-1 in the cerebrospinal fluid, induced by intracerebroventricular injection of a nesfatin-1 antibody, is associated with degeneration of the nigrostriatal dopaminergic system. In combination with evidence that nesfatin-1 mediated the rescue of toxicant induced dopaminergic (DAergic) neuron loss in the substantia nigra (SN), as well as reduced nesfatin-1 levels in the blood of patients with Parkinson's disease (PD), we raise the hypothesis that nesfatin-1 may be essential for the survival of DAergic neurons in SN in mice. In the present study, we found that whole-body *Nucb2* knockout via CRISPR/Cas9 technology in mice led to nigrostriatal dopaminergic system degeneration, as evidenced by a reduction in tyrosine hydrolyses-immunoreactivity neurons in the SN, decreased levels of dopamine and its metabolites in the striatum, and mitochondrial and nuclear impairment in the SN. The underlying mechanism may involve oxidative stress and neuroinflammation induced by down-regulation of circadian rhythm-related gene expression. Furthermore, Nucb2 deletion in mice leads to intestinal microecological imbalance, disorder of the bacterial community structure, metabolic homeostasis disruption, and decreased abundance of some sleep rhythm-related bacterial communities and metabolites. Our findings reported that nesfatin-1 plays a role in maintaining the normal function of the nigrostriatal dopaminergic system, which may provide new therapeutic targets for PD.

Introduction

Dopaminergic (DAergic) neurons are the main source of central neurotransmitter dopamine(DA)¹, which is mainly distributed in the substantia nigra (SN) dense part of the midbrain, and a small part is located in the retina, olfactory bulb and autonomic ganglion². The impairment of DAergic neurons function is associated with Parkinson's disease (PD), a common neurodegenerative disease in the elderly³. The main pathological feature of PD is the degeneration of DAergic neurons in the midbrain SN⁴, which results in the reduction of DA released from the SN to the neuronal endings of the dorsal putamen of the striatum (Str)⁵, resulting in motor symptoms such as muscle rigidity, static tremor and postural gait disorder^{6, 7}. The brain-gut axis is the connection between the central nervous system and the intestine through the vagus nerve. Before the onset of typical motor symptoms, PD patients often have non-motor symptoms, such as gastrointestinal dysfunction and emotional disorders⁸. More than 80% of PD patients have gastrointestinal symptoms such as constipation in the early stage⁹. In addition, pathological changes of PD were also found in the peripheral nervous system such as vagus nerve and intestinal nerve, suggesting that the brain-intestinal axis plays an important role in the pathogenesis of PD^{10, 11}.

Brain-gut peptides are proteins distributed in the central and intestinal regions, including various gastrointestinal hormones secreted by intestinal endocrine cells. As an important component of braingut axis, the role of brain-gut peptides in the pathogenesis of PD has gradually attracted attention.

Nucleobindin2 (*Nucb2*) gene is located on chromosome 7F1 and consists of 14 exons in mice (chromosome 11 in human), with a genomic sequence of 36,186 bp. Post-transcription modifications lead to an mRNA sequence of 1,697 bp with a polypeptide 420 amino acids long¹². The *Nucb2* precursor protein is posttranslationally cleaved by the enzyme prohormone convertase into three peptides, termed nesfatin-1, nesfatin-2 and nesfatin-3¹³. The current study found that only nesfatin-1, which contains 82 amino acids, has biological activity involved in regulating and inhibiting feeding behavior¹⁴. Nesfatin-1 is mainly secreted by X/A-like cells in gastric fundus¹⁵, a small amount of nesfatin-1 is also expressed in peripheral fat, gastroduodenal submucosa and hypothalamic nuclei in the central nervous system^{16, 17}. In addition to inhibiting food intake and regulating energy balance, nesfatin-1 is also involved in cognitive and reproductive regulation, as well as the occurrence of central nervous system diseases such as anxiety, depression and epilepsy^{18–21}. Endogenous nesfatin-1 can pass through the blood-brain barrier to the brain in an unsaturated form²². Some studies have found that nesfatin-1 play an anti-inflammatory and anti-apoptotic role in the central nervous system^{23, 24}, which gradually draws people's attention to the potential neuroprotective effects of nesfatin-1.

Previous work from our group have demonstrated that nesfatin-1 could antagonize rotenone and 1-methyl-4-phenyl-1,2,3,6-tetrahydropyridine (MPTP) induced DAergic neurons degeneration both in vivo and in vitro via anti-apoptotic effects^{25, 26}. By using the patch clamp technique, we found that nesfatin-1 could directly decrease the excitability of nigral DAergic neurons in rat brain slices, suggesting that the nesfatin-1 receptor might be expressed in nigral DAergic neurons²⁷. In 2019, Turkish researchers found that the serum nesfatin-1 level decreased in patients with PD²⁸. Based on the above data, we raised the hypothesis whether the level of nesfatin-1 in the central milieu is critical in maintaining the normal physiological function of the nigrostriatal system. In 2021, we demonstrated that ventricular administration of anti-nesfatin-1 antibody in mice, which lead to reduction of nesfatin-1 levels in the cerebrospinal fluid, could induce nigrostriatal DAergic system degeneration, as well as mitochondrial damage and cell apoptosis were implicated in the underlying mechanism²⁹. Here, we will further test this hypothesis using *Nucb2* knockout C57BL/6J mice.

Several studies have shown that the gut microbiota of patients with PD and animal models have undergone significant changes, indicating a close relationship between PD and the composition and function of the gut microbiota³⁰. For instance, some beneficial bacteria, such as short-chain fatty acids producing bacteria, have experienced a notable decrease in abundance in PD³¹. Mice that received fecal transplants from PD patients exhibited PD-specific motor function deficits, with reduced DAergic neurons in the SN region, intestinal inflammation, damaged intestinal barrier, and aggregation of alphasynuclein in the intestine, suggesting that the pathology of PD may gradually spread from the intestine to the brain³². Additionally, the dysregulation of the gut microbiota can also alter its metabolites, such as acetylcholine, serotonin, and dopamine, short-chain fatty acids (SCFAs), etc., disrupting the balance of inflammation and indirectly influencing the progression and pathogenesis of PD. Therefore, we will study

the alteration in intestine microbiota following *Nucb2* deletion and their relationship with nigrostriatal DAergic system degeneration.

In the present study, we aimed to study (1) Whether the reduction in endogenous nesfatin-1 levels following whole-body *Nucb2* deletion via CRISPR/Cas9 gene editing technology causes lesions in DAergic neurons of the substantia nigra (SN), and to further determine whether nesfatin-1 is involved in maintaining the normal physiological functions of the nigrostriatal system; (2) the alteration of intestine microbiota and metabonomics after *Nucb2* deletion at the whole body level in mice.

Materials and Methods

Ethics statement

Mice were handled in accordance with 'Guide for the Care and Use of Laboratory Animals' and the 'Principles for the Utilization and Care of Vertebrate Animals'. All experiments were approved by the Ethical Committee of Medical College of Qingdao University (QDU-AEC-2021329).

Antibodies

Rabbit polyclonal anti-TH: Cat# Ab6211, Abcam. Rabbit monoclonal anti-Clock: Cat# AB3517, abcam. Mouse monoclonal anti-Bmal1: Cat# sc-365645, Santa Cruz. Rabbit monoclonal anti-Cry2: Cat# 13997-1-AP, Wuhan Sanying. Rabbit monoclonal anti-Dbp: Cat# 16922-1-AP, Wuhan Sanying. Rabbit monoclonal anti-GAPDH: Cat# A19056, Abclonal. HRP Rabbit polyclonal to beta Tubulin: Cat# Ab21058, Abcam. Mouse monoclonal anti-ZO-1: Cat# sc33725-AC, Santa Cruz. Biotinylated goat anti-rabbit IgG: Cat# ab64256, abcam. HRP-conjugated goat anti-mouse IgG (H + L): Cat# AS003, Abclonal. HRP-conjugated goat anti-rabbit IgG secondary antibody: Cat# PI31460, Pierce.

Animals and treatment

 $Nucb2^{-/-}$ mice (T028634) were constructed by CRISPR/Cas9 gene editing technology (GemPharmatech, Shanghai, China). According to the structure of Nucb2 gene, exon4-exon8 of Nucb2-201 (ENSMUST00000032895.14) transcript is used as the knockout region with C57BL/6J mice as genetic background. The region contains 616 bp coding sequence. The F1 heterozygous mice weighing (20 \pm 2) g and aged 8–10 weeks were mated at a 1:2 male/female ratio and kept at constant temperature (22 \pm 2) $^{\circ}$ C in a quiet environment with alternating day and night light (12–12 hrs), drinking and feeding freely. The offspring genetic identification were identified by Quantitative PCR at 3 weeks of age. A53T mice were purchased from Shulaibao Biotechnology Co., Ltd (Wuhan, China).

Mice were selected and housed in a temperature-controlled room under a 12-h light/12-h dark cycle, with free access to deionized water and pellet rat chow. The experiment was conducted using 3-month-old and 6-month-old *Nucb2*^{-/-} male mice, as well as their littermate wild-type (WT) male mice. After motor

behavior and colonic motility testing, mouse plasma was collected for Enzyme-linked immunosorbent assay (ELISA). The left side of the brain was fixed in 4% paraformaldehyde (PFA) for immunofluorescence staining. The right side of the SN was isolated to conduct transcriptomics, western blotting and quantitative Polymerase Chain Reaction (qPCR). Str was isolated for the measurement of DA and its metabolite (homovanillic acid, HVA; dihydroxyphenylacetic acid, DOPAC) contents by high-performance liquid chromatography (HPLC). Intestinal contents were collected for microbiota analysis and metabonomics, as well as colon was isolated for immunohistochemistry.

Genetic identification

To identify the genotype of mice, the tail of newborn mice was clipped at one month of age. The tails of 3 mm to 5 mm were extracted and completely immersed in 500 μ L lysate which containing 1 M Tris-HCL (PH = 8.0), 0.5 M EDTA, 10% SDS, 5 M NaCl and Proteinase K (RPROPK-RO, Roche). Then DNA was extracted and amplified by PCR (primer sequences: F1: GATGGAACCTGGAACTTTCTGC, R1:ATATCCCTAACTGGCCTGGAAC; F2:GAGTACAGCAATGGCAAGCATG, R2:ATGTGTCCACTGTCGAAC). Then Gel electrophoresis was performed with 2% agarose gel at 300 mA current, bands were observed in GIS gel image processing system (Tanon, Shanghai China). WT mice was with one clear band at 417 bp, homozygous $Nucb2^{-/-}$ mice was with one band at 349 bp, and heterozygous $Nucb2^{+/-}$ mice with two bands (Fig. 1a).

Quantitative PCR for nesfatin-1 in the SN and Str

The RNA was extracted by E.Z.N.A.® Total RNA Kit I (R6834, omega). $4\times gDNA$ wiper Mix and $5\times HiScript$ QRT SuperMix (R223-01, Vazyme) were added for reverse transcription reaction. Primer sequences (Forward: ACAAGACCAAAGTACACAACAC; Reverse: CGCTCCTTATCTCCTCTATGTC) for transcripts were designed with Primer Express Software. Quantitative analysis was performed using ChamQ Universal SYBR qPCR Master Mix (Q711-02, Vazyme). Fold induction of gene expression with *Nucb2* was analyzed with the $\Delta\Delta$ Ct method. The Δ Ct is the Ct value of *Nucb2* for the sample normalized to the endogenous housekeeping gene GAPDH transcript.

Enzyme-linked immunosorbent assay for nesfatin-1 in the plasma

The mice were deeply anesthetized and the eyeballs were quickly removed with eye tweezers. Then the blood plasma was carefully collected in the eppendorf tube and stored in the refrigerator at -80 °C. Nesfatin-1 protein content in plasma was detected with the Mouse Nesfatin-1 (Nesfatin-1) ELISA Kit (YJ03288, Shanghai Enzyme Linked Biotechnology). The plasma was diluted 1:5 with the sample diluent. Absorbance values were measured at 450 nm wavelength, a standard curve was drawn and plasma sample concentrations were calculated.

Rotarod test

Motor coordination and balance were assessed using a rotarod apparatus (LE8205, RWD Life Science, China)³³. After being trained for 3 days, mice were placed on the rolling rod with an initial speed of 4 rpm and an accelerating speed levels (4 to 40 rpm in 5 min) mode of the experimental apparatus. Then, three trials with an interval trial time of 2 hrs were performed. The mean latency to fall off the rotarod was recorded to reflect the motor balance ability of mice.

Open field test

Open field test was used to detect the autonomic motor ability of mice, and detect whether mice have anxiety and depression-like emotions³⁴. The mice were placed in an acrylic box (63008, RWD Life Science) with the top open, and the total activity distance, residence time in the center of the open field and average movement speed of the mice within 10 minutes were observed and recorded by the infrared camera. The data analysis was conducted by SMART3.0 software (Panlab, Spain).

Colonic motility test

Constipation is one of the common non-motor symptoms in Parkinson's disease³⁵. Fecal frequency and fecal water content were measured to evaluate the symptoms of constipation. A clean dry squirrel cage was prepared and the defecation of each mouse was observed within 1 hr. Fecal particles of each squirrel cage were collected in the eppendorf tube. After weighing, the weight of the eppendorf tube was subtracted to obtain the wet weight of fecal matter, and the fecal quantity was the fecal frequency. Put the eppendorf tube with the lid open in the oven to dry, weigh the weight of the ependorf tube and subtract the dry weight of the feces. Fecal water content = (fecal wet weight-fecal dry weight)/fecal wet weight.

Immunofluorescence and immunohistochemistry staining

Brains were fixed in 4% PFA for 72 hrs at 4 °C, followed by incubation in 0.1 M phosphate buffer (PBS, pH 7.4) containing 25% sucrose at 4 °C for 3 days. The frozen brain tissues were cut into 25-µm-thick sections. Brain tissue sections were used for immunofluorescence staining of the SN, and for immunohistochemical staining of the Str. After blocking with 10% goat serum (SL038, Solarbio), the sections were incubated overnight at 4 °C with anti-TH (Abcam, 1:1000) in PBS containing 0.1% Triton X-100. Sections used for staining of the SN were incubated with Alexa Fluor 555 donkey anti-rabbit as the secondary antibody (Invitrogen, 1:500), and images were obtained by immunofluorescence microscopy (Observer A1, Zeiss, German). Sections used for staining of the Str were incubated with biotinylated goat anti-rabbit IgG (Abcam, 1:2000) for 1 hrs at 37 °C, followed by amplification with streptavidin peroxidase for 1hrs at 37 °C. Diaminobenzidine hydrogen peroxide (0.01%) was used as the chromogen, and digital images were obtained using a camera.

TH neuron count

The number of tyrosine hydroxylase (TH)-immunoreactivity (TH+) neurons was counted by applying the optical fractionator unbiased stereological method using a fluorescence microscope (Olympus) with MBF Stereo Investigator software. Immunostained cells were counted by an investigator in every 6th sections. For each section, the boundaries of the regions were delineated at low magnification (×10) and counting was conducted at high magnification (×40).

Quantification of DA and its metabolite levels in Str by HPLC

The DA and its metabolites (DOPAC and HVA) levels in the striatal were tested with a previously described method^{36, 37}. Separation was processed on a PEC18 reversed-phase column. The mobile phase (20 mM chromatic acid, 50 mM sodium caproate, 0.134 mM EDTA·2Na, 3.75 mM sodium octane sulfonic acid, 1 mM di-sec-butylamine and containing 5% (v/v) methanol) was used at a flow-rate of 0.6 mL/min. An ACQUITY UPLC (Waters, USA) was employed and operated in screen mode.

Morphological examination of mitochondria and nuclei in SN by transmission electron microscopy

The subcellular microstructure was observed using a JEOL JEM-1400 transmission electron microscope (JEOL, Tokyo, Japan) at Zhongke Baice Testing Technology Co., Ltd. Samples of SN were dice into 2 mm³ particles, fixed with 2.5% glutaraldehyde for 5 hrs, postfixed with 2% osmium tetroxide in Sorensen's buffer for 1 hrs, dehydrated in anascending ethanol series (30, 50, 70, 80, 90, 95, and 100%), and embedded in Epon/Araldite resin. Sections (70 nm) were cut using a Leica EM UC7 Ultramicrotome (Leica Microsystems, Wetzlar, Germany) and placed on 100 mesh copper grids (Electron Microscopy Sciences, Hatfield, PA, United States). Sample grids were poststained with premixed solutions of uranyl acetate and lead citrate (Ultrostain I and II, respectively, Leica Microsystems, Wetzlar, Germany) and examined at 80k Vusinga JEOL JEM-1400 transmission electron microscope (JEOL,Tokyo, Japan). The images were recorded by a TVIPS F416 4k 4k CCD camera running EM-MENU 4.0 acquisition software (Tietz Video and Image Processing Systems, Gauting, Germany)^{29, 38}. The morphology of the nuclei and mitochondria in DAergic neurons was observed and described.

Quantitative PCR for mitochondrial dynamics related gene in the SN

The primer sequences are as follows: MFN1 (Forward: 5'-AACTTGATCGAATAGCATCCGAG-3'; Reverse: 5'-GCATTGCATTGATGACAGAGC-3'). MFN2 (Forward: 5'-CCAACTCCAAGTGTCCGCTC-3'; Reverse: 5'-GTCCAGCTCCGTGGTAACATC-3'). OPA1 (Forward: 5'-CGACTTTGCCGAGGATAGCTT-3'; Reverse: 5'-CGTTGTGAACACACTGCTCTTG-3'). DRP1 (Forward: 5'-CAGGAATTGTTACGGTTCCCTAA-3'; Reverse: 5'-CGTTGTGAACACACTGCTCTTG-3').

CCTGAATTAACTTGTCCCGTGA-3'). FIS1 (Forward: 5'-AGGCTCTAAAGTATGTGCGAGG-3'; Reverse: 5'-GGCCTTATCAATCAGGCGTTC-3').

Transcriptome sequencing

Total RNA was extracted from SN tissues using TRIzol reagent (15596026CN, Invitrogen). The RNA concentration and purity were measured using NanoDrop 2000 (Thermo Fisher). The integrity of RNA was accurately detected using the Agilent Bioanalyzer 2100 system (Agilent). Sequencing libraries were generated using Hieff NGS Ultima Dual-mode mRNA Library Prep Kit for Illumina (Yeasen Biotechnology) following manufacturer's recommendations and index codes were added to attribute sequences to each sample. PCR products were purified (AMPure XP system) and library quality was assessed on the Agilent Bioanalyzer 2100 system. After the library was qualified, high-throughput sequencing platform Illumina NovaSeq 6000 (Illumina) was used for sequencing according to PE150 mode. The sequencing reads were obtained by Illumina Casava (v1.8) software (Illumina). Quantification of gene expression levels were estimated by FPKM (Fragments Per Kilobase of transcript per Million fragments mapped). In the process of differentially expressed genes (DEGs) detection, Fold Change ≥ 1.5 and P value < 0.01 were used as screening criteria. We used cluster Profiler software to test the statistical enrichment of DEGs in Kyoto Encyclopedia of Genes and Genomes (KEGG) pathways. R software (version 4.0.3) was used for data analysis.

Western Blotting for circadian rhythms related gene in the SN

100 μ L protein lysate (RIPA lysate: protease inhibitor: phosphatase inhibitor = 97:2:1) was added to an eppendorf tube containing mouse SN tissue. Centrifuge in supercentrifuge (Centrifuge 5810R, Eppendorf) and draw 80 μ L supernatant into new eppendorf tube. Add 20 μ L of 5×loading buffer to the protein sample, mix well, heated at 100 °C for 10 min, and stored at -80 °C. Antibodies to Clock (Abcam, 1:1000), Bmal1 (Santa, 1:500), Cry2 (Wuhan Sanying, 1:1000), Dbp (Wuhan Sanying, 1:1000), GAPDH (Abclonal, 1:10000), Tublin (Abcam, 1:10000), anti-mouse secondary antibody (Abclonal, 1:10000) and anti-rabbit secondary antibody (Pierce, 1:10000) were used at the dilutions specified by the manufacturer. Densitometry analysis was performed using the ImageJ Gel Analysis tool (Analytik Jena AG).

Quantification of IL-18 and IL-1β in the SN by ELISA

The SN was homogenized in homogenate buffer (0.1% PBS) and diluted 1:10 with the sample dilution buffer (1% BSA with 0.05% Tween-20). Levels of IL-18 and IL-1 β in the SN were determined by the Mouse IL-18 (Interleukin 18) ELISA Kit (ab216165, Abcam) and the Mouse IL-1 β (Interleukin 1 Beta) ELISA Kit (M0037, Elabscience).

Quantification of SOD and MDA in the SN

Weigh the SN tissue accurately and prepare tissue homogenate by adding physiological saline to eppendorf tubes at a weight-to-volume ratio of 1:9 (g/mL). Levels of superoxide dismutase (SOD) and

malondialdehyde (MDA) in the SN were determined by the SOD detection kit (A001-3-2, Nanjing Jiancheng Bioengineering Research Institute) and MDA detection kit (A003-1-2, Nanjing Jiancheng Bioengineering Research Institute).

HE staining and histopathological scoring of colon tissue

The colon of the mice was fixed with 4% PFA overnight, embedded in paraffin, sectioned, and deparaffinized to water. Then, it was stained with hematoxylin and eosin, dehydrated with gradient alcohol, transparented with xylene, and sealed with neutral gum. The tissue images were observed under an optical microscope (BX53F2, OLYMPUS, Japan), and histopathological examination was conducted. Each slide was observed under the light microscope for 3 fields of view, and a semi-quantitative score of 0–4 was given based on three indicators: inflammatory cell infiltration, lesion depth, and degree of crypt disruption, and the total score was calculated.

Determination ZO-1 expression in colonic tissues by immunohistochemistry

The colonic segment extending from the ileocecum to the anus was excised and fixed in 4% PFA. Following fixation, tissues underwent dehydration, embedding, sectioning. Paraffin-embedded sections were dewaxed using an eco-friendly dewaxing solution, absolute ethanol, and distilled water. Antigen retrieval was conducted via microwave irradiation in citrate-based antigen retrieval buffer under the following conditions: Medium-high power: 8 minutes, Standing period: 8 minutes, Medium-low power: 7 minutes. After cooling to room temperature, sections were immersed in 3% hydrogen peroxide for 25 minutes to quench endogenous peroxidase activity. Following thorough rinsing, sections were incubated overnight with primary antibody against ZO-1 (Santa, 1:200). Incubation with HRP-conjugated goat antirabbit IgG secondary antibody (Pierce, 1:1000) for 50 minutes and DAB chromogenic development, Nuclear counterstaining with hematoxylin, Dehydration and mounting, the ZO-1 protein expression patterns were finally examined under a light microscope (BX53F2, OLYMPUS, Japan). The average Optical Density was performed by ImageJ Gel Analysis tool.

16S rDNA amplicon sequencing

After euthanasia, the entire intestinal tract of mice was rapidly excised. Intestinal lumen contents were scraped and transferred into sterile centrifuge tubes. The collected biological samples were flash-frozen in liquid nitrogen and stored at -80°C for subsequent analysis. Sequencing services were commissioned to Beijing Biomarker Technologies Co., Ltd.

16S rDNA Amplicon Sequencing Protocol: Total genomic DNA was isolated from samples. Primers targeting the bacterial-specific region (F:ACTCCTACGGGAGGCAGCA; R:GGACTACHVGGGTWTCTAAT) with sequencing adapters were used for PCR amplification. The PCR products were purified, quantified and homogenized to form sequencing libraries. Qualified libraries were sequenced on the Illumina NovaSeq 6000 platform. Raw data underwent preprocessing (quality filtering, denoising). Processed data were subjected to ASV (Amplicon Sequence Variant) analysis. Taxonomic annotation and diversity

analysis were performed using the SILVA database. Gut microbiota composition, structural features and function were characterized.

Non-Targeted Metabolomics

Appropriate extraction buffer and magnetic beads were added to samples and homogenization via grinding and ultrasonication was conducted. Supernatant was collected after centrifugation and vacuum-dried. Dried extracts were reconstituted for instrumental analysis. The detection platform is the Waters Acquity I-Class PLUS ultra-performance liquid chromatography tandem with the Waters Xevo G2-XS QTOF high-resolution mass spectrometer. The collected raw data were processed through Progenesis QI software for peak extraction, peak alignment and other data processing. The Progenesis QI software was used for identification in the METLIN database, public database and self-built database, and fragment identification was carried out to screen out the metabolites with differences and analyze their metabolic pathways.

Statistical treatment

SPSS 26.0 (IBM, Chicago, IL,USA) was used to analyse the data and GraphPad Prism 11 (Dotmatics, Boston, MA) was used to plot the data. Data were presented as mean ± SEM. *P* < 0.05 was considered to be statistically significant. In Fig. 1b-d, values were analyzed using a two-way ANOVA with a post hoc false discovery rate < 0.05. In Fig. 2b, c, d, f, h, i, j, statistics were also calculated using a two-way ANOVA with a post hoc false discovery rate < 0.05. In Fig. 3c, e, f, g, data were analyzed using a two-way ANOVA with a post hoc false discovery rate < 0.05. In Fig. 4c-g, Fig. 5e-l and Fig. 6b,d, values were analyzed using a two-tailed t-test. In Fig. 7a, b, data were analyzed using a one-way ANOVA with a post hoc false discovery rate < 0.05.

Data availability

All data generated or analyzed during this study are included in this published article (and its supplementary information files). Additional data are available from the corresponding author.

Results

Nucb2 deletion decreased NUCB2 expression in C57BL/6J mice

After NUCB2 deletion, the expression of *Nucb2* mRNA was not detected in the Str, SN and stomach fundus region (Fig. 1. b-d), confirming the absence of *Nucb2* gene in *Nucb2*^{-/-} mice. Despite the efficient deletion of the *Nucb2* gene transcript, nesfatin-1 protein was still detectable in the plasma of *Nucb2*^{-/-} mice (Fig. 1e). Compared with WT mice, the plasma nesfatin-1 levels in *Nucb2*^{-/-} group mice at 3-month-old and 6-month-old decreased by 13.11% and 16.29%, respectively. These results demonstrated that the knockout of *Nucb2* led to a significant reduction in nesfatin-1 levels in C57BL/6J mice.

Nucb2 deletion had no effect on body weight and gastrointestinal motility in mice

Although it has been reported that nesfatin-1 inhibited food intake and thereby reduced body weight³⁹, no significant difference was observed in body weight between WT mice and $Nucb2^{-/-}$ mice at the same age in the present study (Fig. 2b). We further examined the effect of Nucb2 knockout on gastrointestinal motility in mice, results showed that Nucb2 deletion had no significant effect on gastrointestinal motility in $Nucb2^{-/-}$ mice (Fig. 2c, d).

Nucb2 deletion induced motor function disorder in mice

Rotating rod test was conducted to observe the motor balance ability of mice. The longer the mice stay on the rotating rod, the stronger motor balance ability of mice. Compared with WT group, the residence time of 3-month-old and 6-month-old $Nucb2^{-/-}$ mice on rotating rod decreased by 35.54% and 41.08% respectively, indicating that Nucb2 deletion induce a significant decline in the motor balance ability of mice (Fig. 2e, f). Additionally, the rotatod retention time decreased with age in both the $Nucb2^{-/-}$ and WT groups.

The open field test is widely used to assess spontaneous activity in mice. Compared with WT mice, the total distance traveled and mean speed of $Nucb2^{-/-}$ mice showed no significant changes (Fig. 2g-i). However, $Nucb2^{-/-}$ mice exhibited reduced activity in the central zone. The resting time in the central zone of 3-month-old and 6-month-old $Nucb2^{-/-}$ mice decreased by 85.07% and 53.13%, respectively (Fig. 2g, j). These data suggest that Nucb2 deletion has no significant effect on spontaneous activity but induces anxiety-like behavior in mice.

Nucb2 deletion induced nigrostriatal system degeneration in mice

Tyrosine hydroxylase (TH) is an iron-dependent monooxygenase that can hydroxylate tyrosine to DA and is commonly used as a specific marker for detecting DAergic neurons⁴⁰. Compared with that in WT mice, the number of TH+ neurons in the SN of *Nucb2*^{-/-} mice decreased by 33.92% at 3 months of age and 50.23% at 6 months of age (Fig. 3b, c), indicating that *Nucb2* deletion induces DAergic neuron damage in the mouse SN. HPLC was employed to detect the levels of DA and its metabolites HVA and DOPAC in the Str. The levels of DA and its metabolites were decreased in *Nucb2*^{-/-} mice. Compare with WT group, *Nucb2* deletion induced a 38.51% and 25.48% depletion of DA in 3-month-old and 6-month-old mice, respectively (Fig. 3e). The levels of DOPAC and HVA decreased only in 3-month-old *Nucb2*^{-/-} mice, but not in 6-month-old *Nucb2*^{-/-} mice (Fig. 3f, g). The density of TH+ nerve fibers in the Str was reduced in both 3-month-old and 6-month-old *Nucb2*^{-/-} mice (Fig. 3d). These results suggest that *Nucb2* deletion induced nigrostriatal system degeneration in mice.

Nucb2 deletion induced mitochondrial lesions and nuclear shrinkage in SN in mice

Transmission electron microscopy (TEM) were used to observe morphology of nuclei and mitochondria in 3-month-old mice. In the *Nucb2* knockout group, the volume of the nucleus was significantly reduced, as well as the edges of the nucleus were also visibly folded inward, suggesting that the nuclei of

dopaminergic neurons were impaired following *Nucb2* deletion (Fig. 4a). Furthermore, obvious mitochondrial vacuolization was observed in the *Nucb2* knockout group (Fig. 4b). Quantitative real-time PCR (qPCR) was used to detect the expression of mitochondrial dynamic genes. Fis1, which mediates mitochondrial fission, were increased in *Nucb2*^{-/-} mice (Fig. 4c-g).

Circadian rhythms dysfunction was involved in Nucb2 deletion induced nigrostriatal system degeneration in mice

In order to examine possible mechanism by which *Nucb2* deletion might influence DAergic neurons survival, we performed bulk RNA-seg on substantial nigra tissue from 3-month-old and 6-month-old Nucb2-KO mice and WT littermate controls. Exploratory differential gene expression analysis identified a total of 375 differentially expressed genes (DEGs) between the WT group and the Nucb2^{-/-} group at 3month-old mice (Fig. 5a), and 367 DEGs between two groups at 6-month-old mice (Fig. 5c). KEGG pathway analysis was conducted based on DEGs with adjusted P<0.05. Genes differentially expressed between genotypes at both 3-month-old and 6-month-old mice were co-enriched in the circadian entrainment pathway (Fig. 5b, d). These results indicated that circadian entrainment pathway was involved in the Nucb2 deletion induced nigrostriatal system degeneration, which was consistent with previous studies reporting that neuronal deletion of circadian clock genes induced DAergic neurodegeneration via upregulated oxidant stress and inflammation 41, 42. We further assessed the protein expression of circadian related gene via western blot, including Clock, Bmal1, Cry2, and Dbp. The results showed that *Nucb2* deletion down-regulated the protein expression of Clock, Bmal1, Cry2, and Dbp in 3-month-old mice(Fig. 5e-h). It has been reported that circadian clock disruption can cause brain oxidative stress and neuroinflammation 43. We then evaluated the status of oxidative stress and inflammation in *Nucb2* knockout mice; as shown Fig. 5I-L, the levels of SOD, MDA, IL-1β and IL-18 were increased in the SN.

Nucb2 deletion induced intestinal barrier damage

To investigate the impact of *Nucb2* deletion on the intestinal barrier, we performed HE staining and immunohistochemical staining for the tight junction protein ZO-1 on colonic tissues from 3-month-old *Nucb2*^{-/-} mice and WT mice. The WT group exhibited a well-organized colonic structure. In contrast, the *Nucb2*^{-/-} group displayed significant pathological alterations, including extensive inflammatory cell infiltration, increased crypt spacing, and crypt atrophy (Fig. 6a, b). Concurrently, immunohistochemical analysis revealed a significant reduction in ZO-1 protein-positive staining in the *Nucb2*^{-/-} group compared to the WT group (Fig. 6c, d).

Nucb2 deletion induced imbalance of intestinal bacterial community

To investigate the impact of Nucb2 deletion on gut microbiota, we performed 16S rDNA amplicon sequencing on 3-month-old $Nucb2^{-/-}$ mice, WT mice, and A53T mice. A total of 926,253 raw sequences were obtained, and after quality control, denoising, paired-end assembly, and chimera removal, 861,186

high-quality sequences were retained for subsequent analysis. The sequences were processed using the dada2 method in QIIME2 2020.6 software to obtain Amplicon Sequence Variants (ASVs), resulting in 6,310 ASVs. Bacterial community species richness was assessed using the Chao1 index, and community diversity was evaluated using the Shannon index. The Shannon index and Chao1 value showed no significant different among the three groups, indicating that the alpha diversity of gut bacterial community was not affected (Fig. 7a, b). The beta diversity analysis of the bacterial communities was conducted using the Bray-Curtis algorithm for principal coordinates analysis (PCoA). The results showed that the distances between the intestinal microbiota of the three groups of mice were relatively far, indicating that there were certain differences in the intestinal microbiota of the three groups of mice (Fig. 7c). The similarity analysis results based on PERMANOVA/Anosim also indicated that there were significant differences in the Beta diversity among the three groups (*p* < 0.05).

Perform taxonomic annotation of feature sequences using the SILVA reference database, thereby obtaining the community composition of each sample at different classification levels. The mice gut microbiota mainly consists of phyla such as Firmicutes and Bacteroidota. Among them, the relative abundance of Firmicutes in the *Nucb2*^{-/-} group and the A53T group was significantly higher than that in the WT group, while the relative abundances of Bacteroidota and Verrucomicrobiota were significantly lower than that in the WT group. At the genus level, the dominant genus in the WT group was unclassified_*Muribaculaceae*, *Muribaculum*, *Akkermansia*, *Rikenella*, etc., while the community composition in the *Nucb2*^{-/-} group and the A53T group underwent significant changes (Fig. 7d). The results of the significance analysis indicate that relative abundance of unclassified_Lachnospiraceae, *Roseburia*, *Lachnoclostridium*, Lachnospiraceae_UCG_006, *Anaerotruncus*, et al. was significantly increase in the *Nucb2*^{-/-} group and the A53T group, while relative abundance of *Mucispirillum* was significantly decrease (Fig. 7e).

The sample functional abundance was predicted using the PICRUSt2 software. Compared with the WT group, the $Nucb2^{-/-}$ group showed significant changes in functions such as cell motility, signal transduction and metabolism of other amino acids (Fig. 7F). There was no significant difference between the A53T group and the WT group.

Nucb2 deletion induced changes in the metabolic products of the gut microbiota

To perform qualitative and quantitative metabolic profiling of the gut microbiota of 3-month-old *Nucb2*^{-/-} mice, WT mice, and A53T mice, metabonomics was conducted on the LC-QTOF platform. A total of 14,931 peaks were detected, among which 1,868 metabolites were annotated. The results of Principal Component Analysis (PCA) showed that the overall metabolic differences between the *Nucb2*^{-/-} group and the WT group were small, while the differences were significant compared to the A53T group (Fig. 8a). All the identified metabolites were annotated using the KEGG database, and

the differences in metabolites among the groups were analyzed. The results indicated that compared with the WT group, the $Nucb2^{-/-}$ group had 62 different metabolites, of which 30 increased and 32

decreased; compared with the WT group, the A53T group had 441 different metabolites, of which 127 increased and 314 decreased; compared with the $Nucb2^{-/-}$ group, the A53T group had 283 different metabolites, of which 92 increased and 191 decreased (Fig. 8b). Comparing each group pairwise, the logFC results of the top 10 upregulated and downregulated metabolites are shown in Fig. 8c-e. Compared with the WT group, the $Nucb2^{-/-}$ group had increased metabolites such as Hexadecanedioate and Indoxyl, while trans-1,2-Cyclohexanediol and Coenzyme B decreased. The A53T group had increased metabolites such as Phytosphingosine and taurocholic acid, while Ethyl 3-hydroxy hexanoate and Indoline decreased compared with the WT group. Furthermore, the A53T group had increased metabolites such as Phytosphingosine and taurocholic acid, while Ethyl 3-hydroxy hexanoate and Indoline decreased compared with the $Nucb2^{-/-}$ group. The raw intensity of main differential metabolites was shown in Fig. 8F. The concentrations of tryptophan and its indole-related metabolites in the A53T group were significantly reduced. The $Nucb2^{-/-}$ group showed a similar trend, but the difference was not significant. Furthermore, the concentrations of L-methionine and dopamine in the intestines also significantly decreased.

Discussion

The results presented in this study found that (1) *Nucb2* knockout at the whole body level by CRISPR/Cas9 gene editing technology led to nigrostriatal DAergic system degeneration, as evidenced by the reduction in TH + neurons in SN, decreased DA and its metabolites levels in Str, and impaired mitochondria and nuclei in the SN; (2) The underlying mechanism may involve oxidative stress and neuroinflammation induced by downregulation of circadian rhythm-related gene expression; (3) knockout of *Nucb2* in mice leads to intestinal microecological imbalance, disorder of the bacterial community structure, metabolic homeostasis disruption, and decreased abundance of some sleep rhythm-related bacterial communities and metabolites. Taking into account the existing evidence in the literature, i.e., the nesfatin-1-mediated rescue of MPTP-induced DAergic neuron loss in the SN²⁵, the reduction of nesfatin-1 levels in blood in PD patients²⁸, as well as the degeneration of nigrostriatal DAergic system caused by decreased nesfatin-1 level in the CSF by administering anti-nesfatin-1 antibody into the lateral ventricle²⁹, we demonstrated that the brain-gut peptide nesfatin-1 plays a critical role in maintaining the normal function of the nigrostriatal DAergic system.

The main pathological characteristic of PD is the selective loss of dapaminergic neurons in the SN⁴⁴. This results in a reduction in the number of nerve fibers projecting from the substantia nigra to the Str, followed by a decrease in dopamine release in the Str. TH is commonly used as a specific marker for DAergic neurons⁴⁵. DA is a neurotransmitter synthesized by midbrain DAergic neurons^{46, 47}. It can be catalyzed by catecholamine O-methyltransferase to form HVA and oxidized by monoamine oxidase to form DOPAC⁴⁸. We previously reported that diminished nesfatin-1 levels in the CSF after injection of nesfatin-1 antibody into the lateral ventricle likely to led dopamninergic neuron degeneration²⁹. Could the function of midbrain DA neurons be impaired following *Nucb2* knockout, which reduces endogenous

nesfatin-1 expression? Here, immunofluorescence staining was employed to quantify the number of TH⁺ neurons in the substantia nigra of the mouse midbrain, while HPLC was used to measure the levels of DA, HVA and DOPAC in the Str. The results demonstrated that the number of TH⁺ neurons was reduced in both 3-month-old and 6-month-old *Nucb2*^{-/-} mice. HPLC results also revealed that DA and its metabolites in *Nucb2*^{-/-} mice were significantly lower than those in WT mice. Furthermore, subcellular structures such as mitochondria and nuclei in DAergic neurons in SN were severely impaired in *Nucb2*^{-/-} mice. The aforementioned data supported a critical role of nesfatin-1 in the CNS in protecting nigral DAergic neurons against degeneration.

We observed that Nucb2 deletion led to a decline in the motor balance ability of mice in the rotarod test, which may be attributed to Nucb2 deletion-induced DAergic neuron degeneration. Previous studies have described that selective damage to DAergic neurons reduces the duration of high-speed locomotion and rotarod retention time in mice⁴⁹, as well as the signal transduction of DAergic neurons projected to the dorsal Str is related to start/stop signals during locomotion^{50, 51}. The results of the open field test demonstrated that Nucb2 knockout induces anxiety-like and depression-like behaviors in mice, as evidenced by the shorter residence time in the central zone. Previous studies have found that DAergic system is closely related to chronic stress-induced depression⁵². Increased excitability of DAergic neurons is thought to regulate extrasynaptic dopamine levels in response to stressful events $^{53-55}$. Tye et al. demonstrated that selective inhibition of DAergic neurons in the ventral tegmental area (VTA) induces diverse depression-like behaviors in animal models, whereas optogenetic activation of VTA DAergic neurons reverses these phenotypes⁵⁶. Therefore, excitability of DAergic neurons is crucial for the regulation of depression-related behaviors⁵⁷. The specific molecular signaling pathway of dysregulation of DAergic system leading to depression is still unclear. However, studies have also reported that overactivation of DAergic neurons induced by chronic emotional stress can trigger anxiety-like behavioral changes and transient alterations in social interaction⁵⁸. Nesfatin-1 has been observed to exert a regulatory role in anxiety- and depression-like behaviors with inconsistent results. In a recent animal study, rats exposed to continuous stress during early life exhibited anxiety-like behaviors, with elevated nesfatin-1 levels detected in their hippocampus, plasma, and fundus⁵⁹. This suggests that endogenous nesfatin-1 upregulated under stress conditions may play a role in the development of anxiety. A potential link between nesfatin-1 and anxiety has also been identified in human studies. A study involving male patients diagnosed with generalized anxiety disorder reported that nesfatin-1 levels in these patients were 45% lower compared to those in age- and sex-matched healthy controls⁶⁰. Another study reported that plasma nesfatin-1 levels were 33% higher in women with high anxiety compared to those with low anxiety⁶¹. It is important to note that these studies did not assess potential sex differences in the regulation of NUCB2/nesfatin-1, which may contribute to the partial inconsistencies in the aforementioned results. In addition, depression is also a common non-motor symptom of PD⁶², and its mechanism is related to the spread of basal synaptic lesions to the mesencephalic limbic DA system⁶³. The role of nesfatin-1 in central nervous system diseases such as anxiety and depression remains to be further studied.

Circadian rhythm disruptions are common comorbidities of neurodegenerative disorders $^{41, 64}$. Diminished expression of the core clock gene Bmal1 was observed in PD patients 43 . In this study, transcriptome data analysis indicated that circadian rhythm dysregulation is involved in the damage to the midbrain nigrostriatal system induced by Nucb2 deletion. The finding is further validated by the reduced protein expression of circadian rhythm-related genes in the $Nucb2^{-/-}$ mice, as detected by western blotting. This is consistent with previous reports that brain aging was associated with diminished circadian clock output and reduced expression of core clock proteins 65 . Circadian clocks regulated multiple aspects of cellular function, including cellular metabolism, redox homeostasis, and inflammation. Several studies reported that circadian clock disruption accelerates the degeneration of DAergic neurons by regulating the rhythmicity and magnitude of DAergic neurons' vulnerability to oxidative stress, as well as activating neuroinflammation $^{64, 65}$. We further measured the levels of SOD, MDA, IL-1 β and IL-1 β , and demonstrated these markers are up-regulated in SN of $Nucb2^{-/-}$ mice. Together, these data suggested that oxidative stress and neuroinflammation induced by circadian rhythm dysregulation, are involved in the degeneration of nigral DAergic neurons caused by Nucb2 deletion.

Intestine may play an important role in the early stages of PD as PD patients often present with gastrointestinal symptoms before the onset of behavioral symptoms, and there are indeed significant differences in the intestinal flora between patients with PD and healthy individuals^{66, 67}. Our results of HE staining and immunohistochemical analysis indicated that *Nucb2* deletion led to intestinal barrier damage. The 16S rDNA sequencing results of the intestinal microbiota indicated that the microbiota composition, structure and functional genes of the intestinal microbiota in the Nucb2 knockout mice and A53T mice were significantly different from those of the control group. These changes may have certain connections with the onset of PD. For instance, *Mucispirillum* had a lower abundance in the *Nucb2*^{-/-} group and the A53T group, which was consistent with the results of Zhang et al⁶⁸. *Mucispirillum* schaedleri is a type of mucin bacterium in the intestinal microbiota, mainly parasitizing in the intestinal mucosa layer, and can inhibit colitis caused by Salmonella⁶⁹. The decrease in its abundance may weaken this protective effect and increase the risk of infection. Akkermansia also had a significantly reduced relative abundance in the *Nucb2*^{-/-} group and the A53T group. Studies have found that the level of Akkermansia muciniphila in the feces of patients with ulcerative colitis is lower than that of healthy individuals, and oral administration of the Akkermansia muciniphila strain BAA-835 significantly improved the symptoms of acute colitis induced by dextran sulfate sodium (DSS)⁷⁰. Moreover, Akkermansia can regulate the sleep rhythm through the gut-brain axis and help improve sleep disorders and cognitive function impairment caused by sleep deprivation⁷¹. Therefore, the decrease in Akkermansia abundance may aggravate intestinal inflammation, thereby alter the host's circadian rhythm and cause cognitive dysfunction. Lachnoclostridium significantly increased in the Nucb2^{-/-} group, which was consistent with the results of Kim et al⁷². Some studies have also shown that the relative abundance of *Lachnoclostridium* increases in intestinal inflammation lesions, suggesting that the proliferation of *Lachnoclostridium* exacerbates intestinal barrier permeability, allowing inflammatory

factors to enter the central nervous system through the 'gut-brain axis', triggering neuroinflammation and behavioral changes. The intestinal microbiota is highly complex, with hundreds or even thousands of bacterial species involved, and each of them produces a large number of chemical substances that affect the immune system and bodily functions, etc. Therefore, further research is needed to more effectively evaluate the interaction between the host and the intestinal microbiota, in order to provide new personalized therapeutic interventions and preventive strategies targeting the gut-brain axis.

The results of metabolomics analysis indicate that the concentration of tryptophan decreases, and the content of indole substances decreases, suggesting that intestinal flora disorder leads to imbalance in tryptophan metabolism. Studies have shown that abnormal metabolism of tryptophan is related to the pathological mechanisms of various diseases in the central nervous system. Indole metabolites can protect the nervous system and have anti-inflammatory, intestinal barrier repair and other effect⁷³. The decrease in their concentration may be one of the causes of intestinal barrier damage. The concentration of metabolite L-methionine also decreases in this study. L-methionine is a key substrate of the S-adenosylmethionine (SAM) cycle. Its reduction leads to abnormal expression of host clock genes (such as Bmal1, Clock), disrupting the circadian oscillation pattern of metabolic pathways, and resulting in a decrease in metabolic activity during the wakefulness period⁷⁴. Moreover, L-methionine can protect neurons from oxidative imbalance and mitochondrial dysfunction, thereby preventing the progression of neurodegenerative processes⁷⁵. Therefore, the decrease in L-methionine concentration may also be one of the pathogenic mechanisms of Parkinson's disease. Additionally, the results revealed that the concentration of dopamine in the intestine decreases and this may affect the dopamine concentration in the central nervous system through the vagus nerve, thereby promoting the onset of Parkinson's disease⁷⁶.

In summary, our data demonstrated that reducing the nesfatin-1 expression by *Nucb2* knockout at the whole body levels can induce nigrostriatal dopaminergic system degeneration *in vivo*. This effect may be mediated by decreased expression of circadian rhythm-related genes in the SN region and the intestinal microbiota imbalance after *Nucb2* deletion. Our study provides new evidence that nesfatin-1 is involved in maintaining the normal physiological function of the nigrostriatal system.

Declarations

Competing interests

The authors declare no competing interests.

Author Contribution

X.S., and X.K. conceived the project and designed the study. R.S., and S.L. performed the experiments, analyzed data and interpreted results. R.S. wrote the manuscript and R.W. commented on it. X.S., X.K.,

and S.L. reviewed and edited the manuscript. All authors have read and approved the final version of the manuscript.

Acknowledgement

This work was supported by the National Natural Science Foundation of China (82171570).

References

- 1. Tian, L., et al. Roles of Transcription Factors in the Development and Reprogramming of the Dopaminergic Neurons. *Int J Mol Sci.* 23, (2022).
- 2. Tierney, A.J., T. Kim, and R. Abrams Dopamine in crayfish and other crustaceans: distribution in the central nervous system and physiological functions. *Microsc Res Tech.* 60, 325–335 (2003).
- 3. Samii, A., J.G. Nutt, and B.R. Ransom Parkinson's disease. *Lancet.* 363, 1783-1793 (2004).
- 4. Zhu, B., et al. The immunology of Parkinson's disease. Semin Immunopathol. 44, 659-672 (2022).
- 5. Kalia, L.V. and A.E. Lang Parkinson's disease. *Lancet*. 386, 896–912 (2015).
- 6. Mullin, S. and A.H. Schapira Pathogenic mechanisms of neurodegeneration in Parkinson disease. *Neurol Clin.* 33, 1–17 (2015).
- 7. Sharififar, S., et al. The effects of whole body vibration on mobility and balance in Parkinson disease: a systematic review. *Iran J Med Sci.* 39, 318–326 (2014).
- 8. Mrabet, S., et al. Gastrointestinal Dysfunction and Neuropathologic Correlations in Parkinson Disease. *J Clin Gastroenterol.* 50, e85-90 (2016).
- 9. Yemula, N., et al. Parkinson's Disease and the Gut: Symptoms, Nutrition, and Microbiota. *J Parkinsons Dis.* 11, 1491–1505 (2021).
- 10. Scheperjans, F., P. Derkinderen, and P. Borghammer The Gut and Parkinson's Disease: Hype or Hope? *J Parkinsons Dis.* 8, S31-s39 (2018).
- 11. Claudino Dos Santos, J.C., et al. Gut-microbiome-brain axis: the crosstalk between the vagus nerve, alpha-synuclein and the brain in Parkinson's disease. *Neural Regen Res.* 18, 2611–2614 (2023).
- 12. Zhou, Q., et al. NUCB2: roles in physiology and pathology. J Physiol Biochem. 78, 603-617 (2022).
- 13. Schalla, M.A., et al. NUCB2/nesfatin-1 Inhibitory effects on food intake, body weight and metabolism. *Peptides*. 128, 170308 (2020).
- 14. Oh, I.S., et al. Identification of nesfatin-1 as a satiety molecule in the hypothalamus. *Nature*. 443, 709–712 (2006).
- 15. Stengel, A., M. Mori, and Y. Taché The role of nesfatin-1 in the regulation of food intake and body weight: recent developments and future endeavors. *Obes Rev.* 14, 859–870 (2013).
- 16. Kohno, D., et al. Nesfatin-1 neurons in paraventricular and supraoptic nuclei of the rat hypothalamus coexpress oxytocin and vasopressin and are activated by refeeding. *Endocrinology*. 149, 1295–1301

(2008).

- 17. Goebel-Stengel, M. and L. Wang Central and peripheral expression and distribution of NUCB2/nesfatin-1. *Curr Pharm Des.* 19, 6935–6940 (2013).
- 18. Liu, M., et al. Plasma levels of nesfatin-1 as a new biomarker in depression in Asians: evidence from meta-analysis. *Biomarkers*. 25, 228–234 (2020).
- 19. Mori, M., et al. Discovery of nesfatin-1 and overview of biological actions and new developments. *Curr Pharm Des.* 19, 6921–6928 (2013).
- 20. Weibert, E., T. Hofmann, and A. Stengel Role of nesfatin-1 in anxiety, depression and the response to stress. *Psychoneuroendocrinology*. 100, 58–66 (2019).
- 21. Arabacı Tamer, S., et al. Nesfatin-1 ameliorates oxidative brain damage and memory impairment in rats induced with a single acute epileptic seizure. *Life Sci.* 294, 120376 (2022).
- 22. Pan, W., H. Hsuchou, and A.J. Kastin Nesfatin-1 crosses the blood-brain barrier without saturation. *Peptides.* 28, 2223–2228 (2007).
- 23. Erfani, S., et al. Nesfatin-1 Improve Spatial Memory Impairment Following Transient Global Cerebral Ischemia/Reperfusion via Inhibiting Microglial and Caspase-3 Activation. *J Mol Neurosci*. 65, 377–384 (2018).
- 24. Özsavcí, D., et al. The novel function of nesfatin-1 as an anti-inflammatory and antiapoptotic peptide in subarachnoid hemorrhage-induced oxidative brain damage in rats. *Neurosurgery*. 68, 1699–1708; discussion 1708 (2011).
- 25. Shen, X.L., et al. Nesfatin-1 protects dopaminergic neurons against MPP(+)/MPTP-induced neurotoxicity through the C-Raf-ERK1/2-dependent anti-apoptotic pathway. *Sci Rep.* 7, 40961 (2017).
- 26. Tan, Z., et al. Nesfatin-1 antagonized rotenone-induced neurotoxicity in MES23.5 dopaminergic cells. *Peptides*. 69, 109–114 (2015).
- 27. Li, C., et al. Nesfatin-1 decreases excitability of dopaminergic neurons in the substantia nigra. *J Mol Neurosci.* 52, 419–424 (2014).
- 28. Emir, G.K., et al. The association of low levels of nesfatin-1 and glucagon-like peptide-1 with oxidative stress in Parkinson's disease. *Neurol Sci.* 40, 2529–2535 (2019).
- 29. Chen, H., et al. Reduction in Nesfatin-1 Levels in the Cerebrospinal Fluid and Increased Nigrostriatal Degeneration Following Ventricular Administration of Anti-nesfatin-1 Antibody in Mice. *Front Neurosci.* 15, 621173 (2021).
- 30. Salim, S., et al. Gut microbiome and Parkinson's disease: Perspective on pathogenesis and treatment. *J Adv Res.* 50, 83–105 (2023).
- 31. Hilton, D., et al. Accumulation of alpha-synuclein in the bowel of patients in the pre-clinical phase of Parkinson's disease. *Acta Neuropathol.* 127, 235–241 (2014).
- 32. Munoz-Pinto, M.F., et al. Gut-first Parkinson's disease is encoded by gut dysbiome. *Mol Neurodegener*. 19, 78 (2024).

- 33. Lubrich, C., P. Giesler, and M. Kipp Motor Behavioral Deficits in the Cuprizone Model: Validity of the Rotarod Test Paradigm. *Int J Mol Sci.* 23, (2022).
- 34. Kraeuter, A.K., P.C. Guest, and Z. Sarnyai The Open Field Test for Measuring Locomotor Activity and Anxiety-Like Behavior. *Methods Mol Biol.* 1916, 99–103 (2019).
- 35. Du, Y., et al. Probiotics for constipation and gut microbiota in Parkinson's disease. *Parkinsonism Relat Disord.* 103, 92–97 (2022).
- 36. Jia, F., et al. Deubiquitylase OTUD3 prevents Parkinson's disease through stabilizing iron regulatory protein 2. *Cell Death Dis.* 13, 418 (2022).
- 37. Dai, Y., et al. Astrocyte-derived apolipoprotein D is required for neuronal survival in Parkinson's disease. *NPJ Parkinsons Dis.* 10, 143 (2024).
- 38. Eustaquio, T., et al. Electron microscopy techniques employed to explore mitochondrial defects in the developing rat brain following ketamine treatment. *Exp Cell Res.* 373, 164–170 (2018).
- 39. Shimizu, H., et al. Peripheral administration of nesfatin-1 reduces food intake in mice: the leptin-independent mechanism. *Endocrinology*. 150, 662–671 (2009).
- 40. Nagatsu, T. Catecholamines and Parkinson's disease: tyrosine hydroxylase (TH) over tetrahydrobiopterin (BH4) and GTP cyclohydrolase I (GCH1) to cytokines, neuromelanin, and gene therapy: a historical overview. *J Neural Transm (Vienna)*. 131, 617–630 (2024).
- 41. Vallée, A., et al. Circadian rhythms, Neuroinflammation and Oxidative Stress in the Story of Parkinson's Disease. *Cells.* 9, (2020).
- 42. Majcin Dorcikova, M., et al. Circadian clock disruption promotes the degeneration of dopaminergic neurons in male Drosophila. *Nat Commun.* 14, 5908 (2023).
- 43. Kanan, M.F., et al. Neuronal deletion of the circadian clock gene Bmal1 induces cell-autonomous dopaminergic neurodegeneration. *JCI Insight*. 9, (2024).
- 44. Daubner, S.C., T. Le, and S. Wang Tyrosine hydroxylase and regulation of dopamine synthesis. *Arch Biochem Biophys.* 508, 1–12 (2011).
- 45. Steinkellner, T., et al. Role for VGLUT2 in selective vulnerability of midbrain dopamine neurons. *J Clin Invest.* 128, 774–788 (2018).
- 46. Zhou, Z.D. and T.M. Lim Roles of glutathione (GSH) in dopamine (DA) oxidation studied by improved tandem HPLC plus ESI-MS. *Neurochem Res.* 34, 316–326 (2009).
- 47. Masato, A., et al. Impaired dopamine metabolism in Parkinson's disease pathogenesis. *Mol Neurodegener.* 14, 35 (2019).
- 48. Zhang, S., R. Wang, and G. Wang Impact of Dopamine Oxidation on Dopaminergic Neurodegeneration. *ACS Chem Neurosci.* 10, 945–953 (2019).
- 49. Wu, J., et al. Distinct Connectivity and Functionality of Aldehyde Dehydrogenase 1a1-Positive Nigrostriatal Dopaminergic Neurons in Motor Learning. *Cell Rep.* 28, 1167–1181.e1167 (2019).
- 50. Howe, M.W. and D.A. Dombeck Rapid signalling in distinct dopaminergic axons during locomotion and reward. *Nature*. 535, 505–510 (2016).

- 51. Jin, X. and R.M. Costa Start/stop signals emerge in nigrostriatal circuits during sequence learning. *Nature*. 466, 457–462 (2010).
- 52. Baik, J.H. Stress and the dopaminergic reward system. Exp Mol Med. 52, 1879–1890 (2020).
- 53. Grace, A.A. Dysregulation of the dopamine system in the pathophysiology of schizophrenia and depression. *Nat Rev Neurosci.* 17, 524–532 (2016).
- 54. Floresco, S.B., et al. Afferent modulation of dopamine neuron firing differentially regulates tonic and phasic dopamine transmission. *Nat Neurosci.* 6, 968–973 (2003).
- 55. Valenti, O., D.J. Lodge, and A.A. Grace Aversive stimuli alter ventral tegmental area dopamine neuron activity via a common action in the ventral hippocampus. *J Neurosci*. 31, 4280–4289 (2011).
- 56. Tye, K.M., et al. Dopamine neurons modulate neural encoding and expression of depression-related behaviour. *Nature*. 493, 537–541 (2013).
- 57. Zhong, P., et al. HCN2 channels in the ventral tegmental area regulate behavioral responses to chronic stress. *Elife*. 7, (2018).
- 58. Qi, G., et al. NAc-VTA circuit underlies emotional stress-induced anxiety-like behavior in the three-chamber vicarious social defeat stress mouse model. *Nat Commun.* 13, 577 (2022).
- 59. Jing, F.C., et al. Potential rat model of anxiety-like gastric hypersensitivity induced by sequential stress. *World J Gastroenterol.* 23, 7594–7608 (2017).
- 60. Gunay, H., et al. Decreased plasma nesfatin-1 levels in patients with generalized anxiety disorder. *Psychoneuroendocrinology*. 37, 1949–1953 (2012).
- 61. Hofmann, T., et al. NUCB2/nesfatin-1 Is Associated with Elevated Levels of Anxiety in Anorexia Nervosa. *PLoS One.* 10, e0132058 (2015).
- 62. Ffytche, D.H., et al. Risk factors for early psychosis in PD: insights from the Parkinson's Progression Markers Initiative. *J Neurol Neurosurg Psychiatry*. 88, 325–331 (2017).
- 63. Muñoz, A., et al. Interactions Between the Serotonergic and Other Neurotransmitter Systems in the Basal Ganglia: Role in Parkinson's Disease and Adverse Effects of L-DOPA. *Front Neuroanat.* 14, 26 (2020).
- 64. Majcin Dorcikova, M., et al. Circadian clock disruption promotes the degeneration of dopaminergic neurons in male Drosophila. *Nat Commun.* 14, 5908 (2023).
- 65. Musiek, E.S., et al. Circadian clock proteins regulate neuronal redox homeostasis and neurodegeneration. *J Clin Invest*. 123, 5389–5400 (2013).
- 66. Li, Y., et al. Intestinal Inflammation and Parkinson's Disease. *Aging Dis.* 12, 2052–2068 (2021).
- 67. Costa, H.N., et al. Parkinson's Disease: A Multisystem Disorder. *Neurosci Bull.* 39, 113–124 (2023).
- 68. Zhang, P., et al. Specific gut microbiota alterations in essential tremor and its difference from Parkinson's disease. *NPJ Parkinsons Dis.* 8, 98 (2022).
- 69. Herp, S., et al. The human symbiont Mucispirillum schaedleri: causality in health and disease. *Med Microbiol Immunol.* 210, 173–179 (2021).

- 70. Qu, S., et al. Akkermansia muciniphila Alleviates Dextran Sulfate Sodium (DSS)-Induced Acute Colitis by NLRP3 Activation. *Microbiol Spectr.* 9, e0073021 (2021).
- 71. Li, N., et al. Akkermansia muciniphila supplementation prevents cognitive impairment in sleep-deprived mice by modulating microglial engulfment of synapses. *Gut Microbes*. 15, 2252764 (2023).
- 72. Kim, J.E., et al. Compositional changes in fecal microbiota in a new Parkinson's disease model: C57BL/6-Tg(NSE-haSyn) mice. *Lab Anim Res*. 39, 30 (2023).
- 73. Ranhotra, H.S. Discrete interplay of gut microbiota L-tryptophan metabolites in host biology and disease. *Mol Cell Biochem.* 479, 2273–2290 (2024).
- 74. Liu, X., et al. Gut microbial methionine impacts circadian clock gene expression and reactive oxygen species level in host gastrointestinal tract. *Protein Cell.* 14, 309–313 (2023).
- 75. Catanesi, M., et al. L-Methionine Protects against Oxidative Stress and Mitochondrial Dysfunction in an In Vitro Model of Parkinson's Disease. *Antioxidants (Basel)*. 10, (2021).
- 76. Hamamah, S., et al. Role of Microbiota-Gut-Brain Axis in Regulating Dopaminergic Signaling. *Biomedicines*. 10, (2022).

Figures

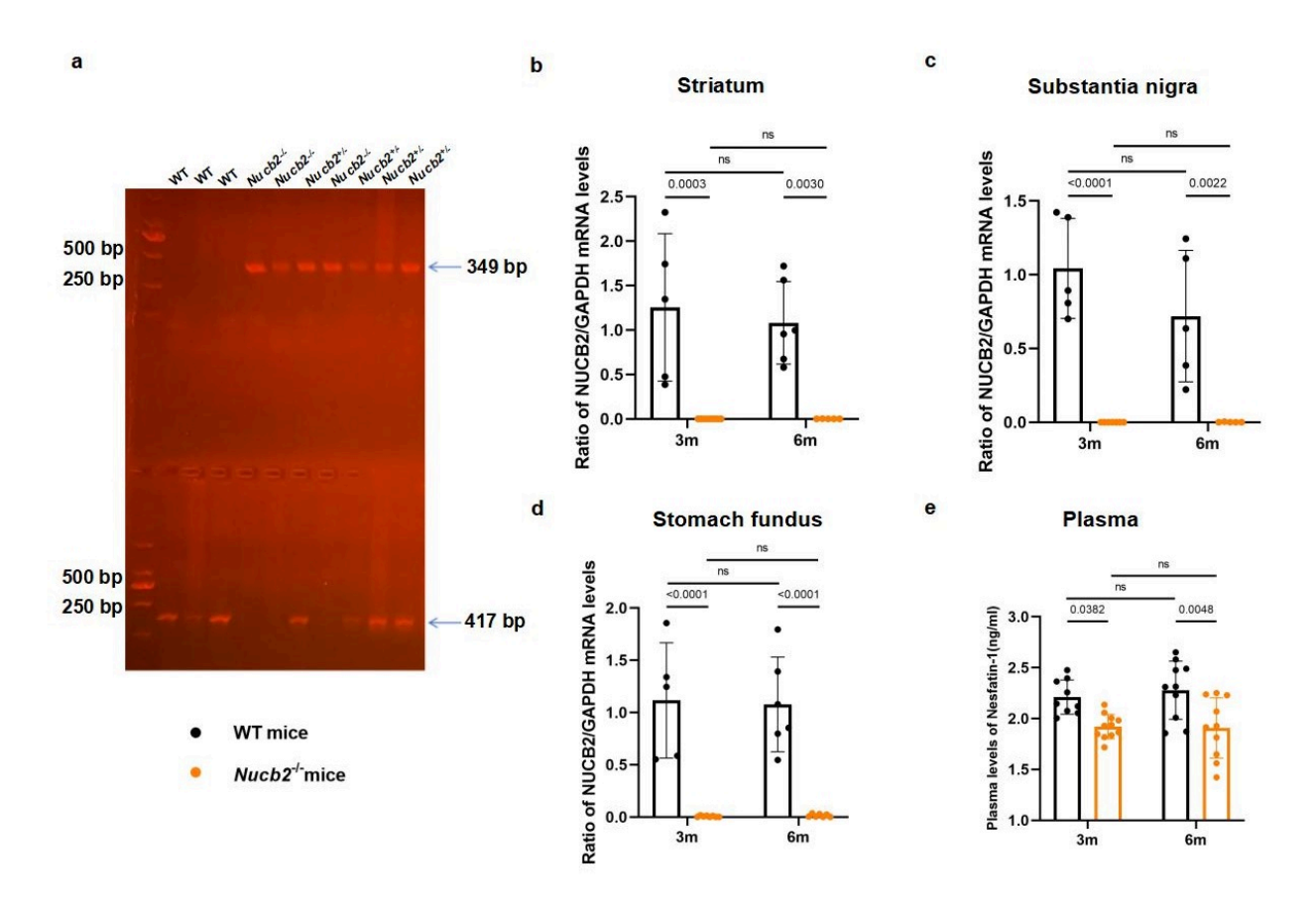


Figure 1

Nucb2 knockout decreased the *Nucb2* expression in mice. **a** Image of genotyping of mouse. WT mice with one band at 417 bp, homozygous $Nucb2^{-/-}$ mice with one band at 349 bp, and heterozygous $Nucb2^{+/-}$ mice with two bands. **b-d** RT-PCR confirmed that the mRNA level of Nucb2 in striatum, substantia nigra, and stomach fundus of $Nucb2^{-/-}$ mice was significantly decreased. **e** ELISA showed that nesfatin-1 levels in the plasma were decreased in $Nucb2^{-/-}$ mice. n = 5-11 mice. Statistics were calculated using two-way ANOVA with a false discovery rate <0.05. **b-e**, Data were presented as mean \pm SEM. Nucb2: nucleobindin-2, 3m: 3-month-old; 6m: 6-month-old; WT: wild-type; $Nucb2^{-/-}$: Nucb2 knockout.

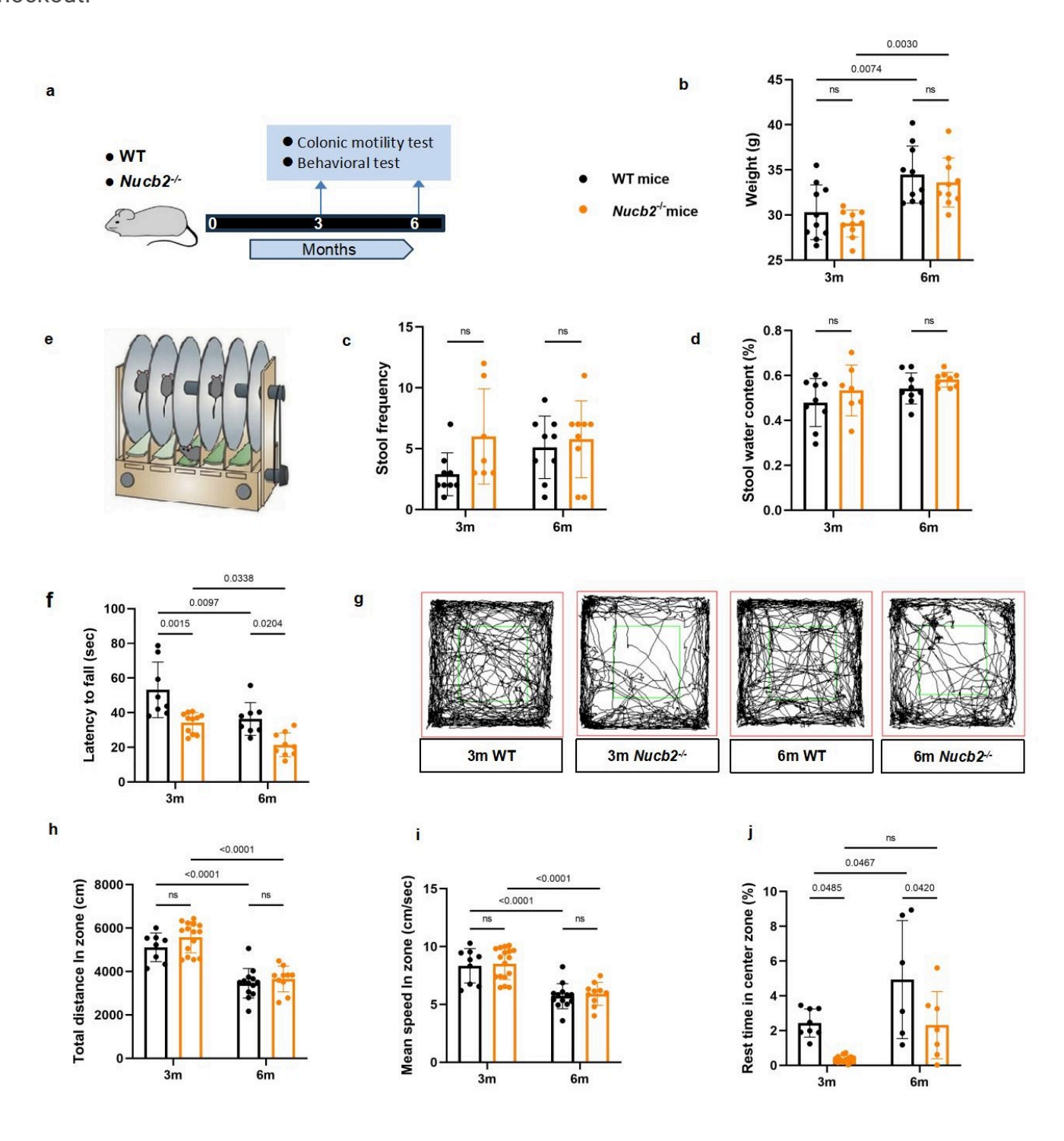


Figure 2

Effects of *Nucb2* deletion on body weight, gastrointestinal motility, and motor function in mice. a Schematic illustration in mice experiment. **b** *Nucb2* deletion has no effect on body weight. **c-d** *Nucb2* deletion has no effect on gastrointestinal motility. **e-f** The rotarod test showed that *Nucb2* deletion shorten the time mice stay on the rotarod. **g-j** The open field test showed a significant decrease in the resting time in the central zone in *Nucb2* mice, compared with that of WT mice. n = 7-15 mice. Statistics were calculated using two-way ANOVA with a false discovery rate. **b**, **c**, **d**, **f**, **h**, **i**, **j** Data were presented as mean ± SEM. 3m: 3-month-old, 6m: 6-month-old, *Nucb2*: nucleobindin-2, *Nucb2* knockout, WT: wild-type.

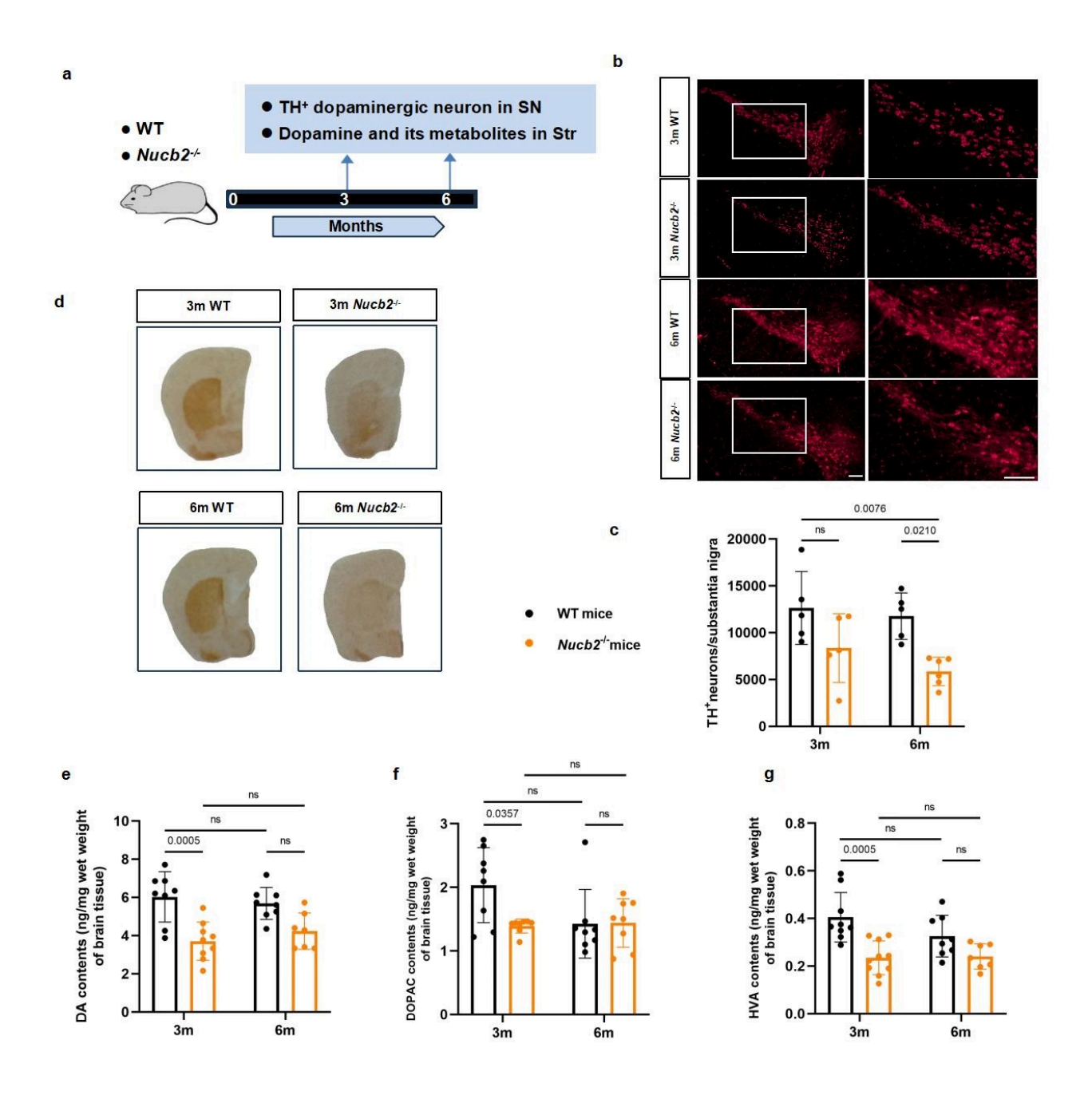
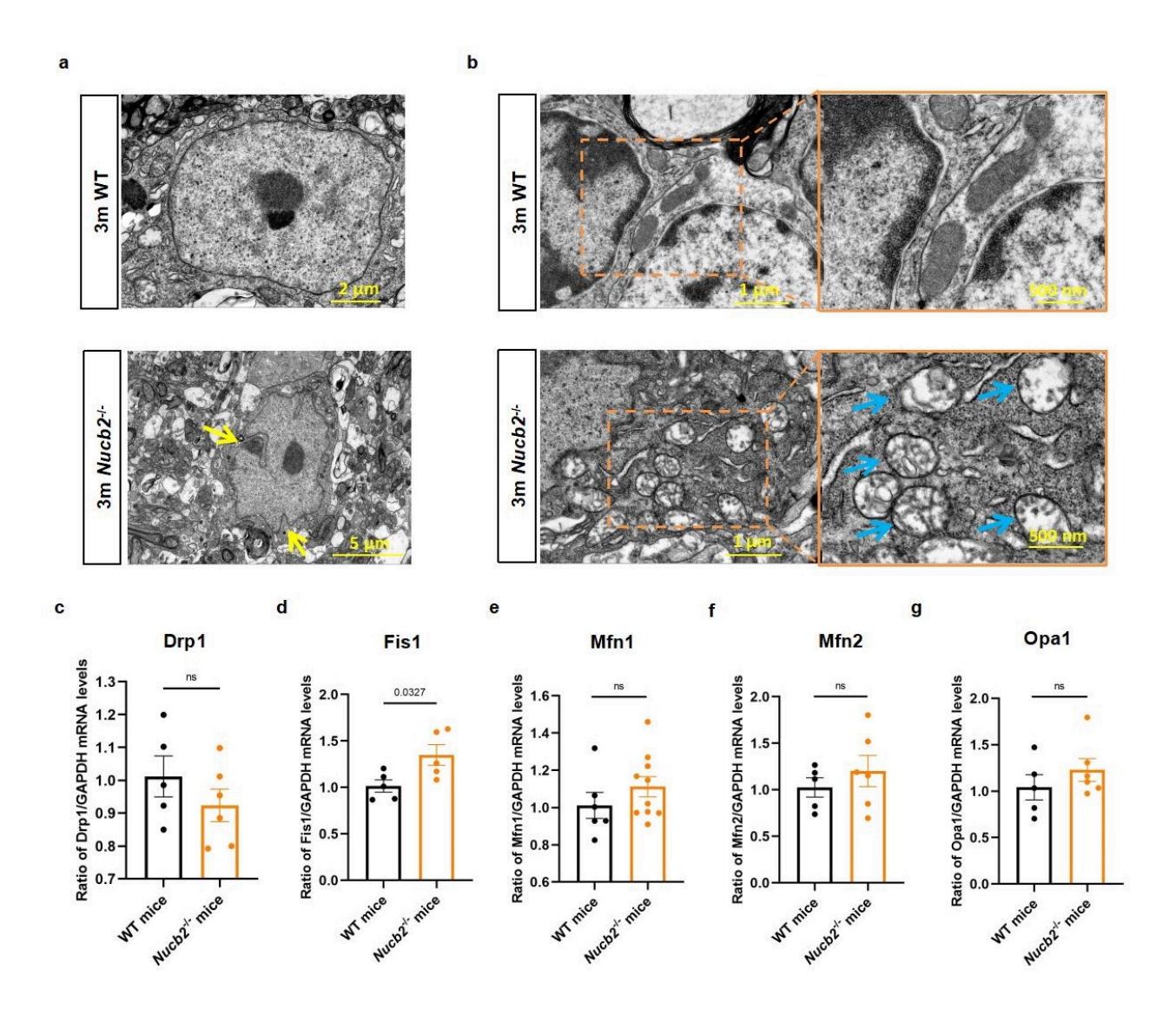
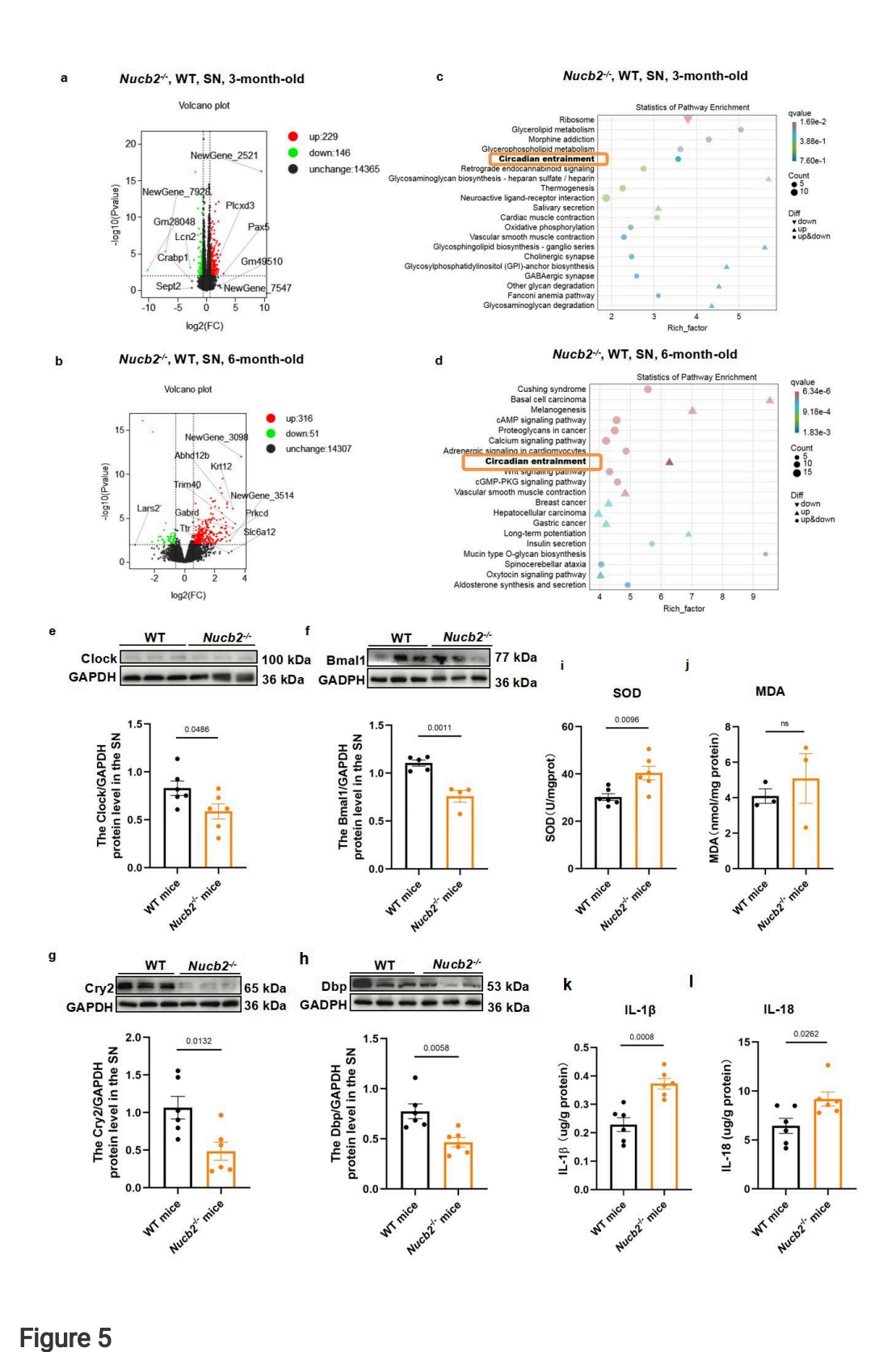


Figure 3



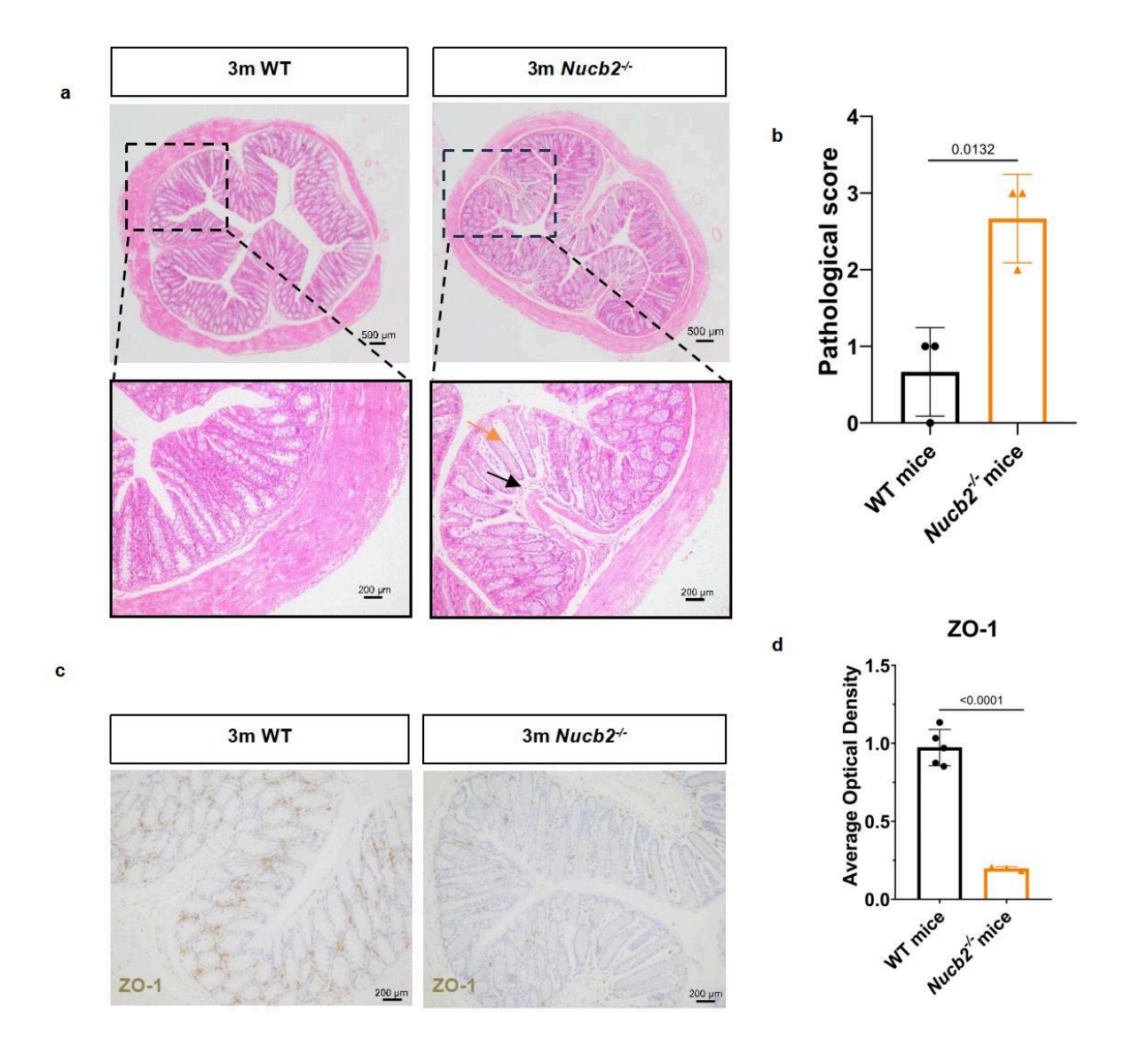
Nucb2 deletion induced mitochondrial lesions and nuclear shrinkage in SN in 3-month-old mice. a *Nucb2* deletion induced nuclear shrinkage, the yellow arrows indicated the shrunken nuclei. b *Nucb2* deletion induced mitochondrial vacuolization, the blue arrows indicated vacuolated mitochondria. **c-g** qRT-PCR analyzed the mRNA levels of Drp1, Fis1, Mfn1, Mfn2, and Opa1 in SN in mice. n = 5-10. Statistics were calculated using a two-tailed *t*-test with a false discovery rate <0.05. **c-g**, Data were presented as mean \pm SEM. *Nucb2*: nucleobindin-2, 3m: 3-month-old, WT: wild-type, *Nucb2*\(^-: Nucb2\) knockout.

Figure 4



Circadian rhythms related-gene was involved in *Nucb2* deletion induced nigrostriatal system degeneration. a Volcano plot showing DEGs in SN from 3-month-old $Nucb2^{-/-}$ mice, as compared with WT mice. n = 3 mice/genotype.b Volcano plot showing DEGs in SN from 6-month-old $Nucb2^{-/-}$ mice. n = 3 mice/genotype.c Exploratory KEGG pathway analysis of all DEGs in SN samples from 3-month-old

Nucb2^{-/-} mice (P< 0.05). **d** KEGG pathway analysis of all DEGs in SN samples from 6-month-old *Nucb2*^{-/-} mice (P< 0.05). **e-h** Western blotting confirmed decreased expression of circadian rhythms-related gene in 3-month old *Nucb2*^{-/-} mice. **i, j** *Nucb2* deletion up-regulated the levels of SOD and MDA in SN sample from 3-month-old mice. **k, l** ELISA results showed that *Nucb2* deletion up-regulated the levels of IL-18 and IL-1β in SN sample from 3-month-old mice. n = 3-6 mice. Statistics were calculated using a two-tailed *t*-test with false discovery rate <0.05. **e-l**, Data were presented as mean ± SEM. 3m: 3-month-old, DEGs: differentially expressed genes; *Nucb2*: nucleobindin-2, *Nucb2*^{-/-}: *Nucb2* knockout, SN: substantia nigra, WT: wild-type.



NUCB2 deletion induced inflammation and intestinal barrier damage. a Histological analysis [hematoxylin and eosin (H&E)] of the colon sections. The black arrows indicate the infiltration of

inflammatory cells, the orange arrows represent the increase in the distance between the crypts and the atrophy of the crypts. **b** Histological scores of different groups. **c** Immunohistochemical analysis for ZO-1 in different groups. **d** The average optical density of ZO-1 positive area in different groups. n = 3. Statistics were calculated using a two-tailed *t*-test with false discovery rate <0.05. **b**, **d**, Data were presented as mean \pm SEM. *Nucb2*: nucleobindin-2, 3m: 3-month-old, WT: wild-type, *Nucb2*/-: *Nucb2* knockout.

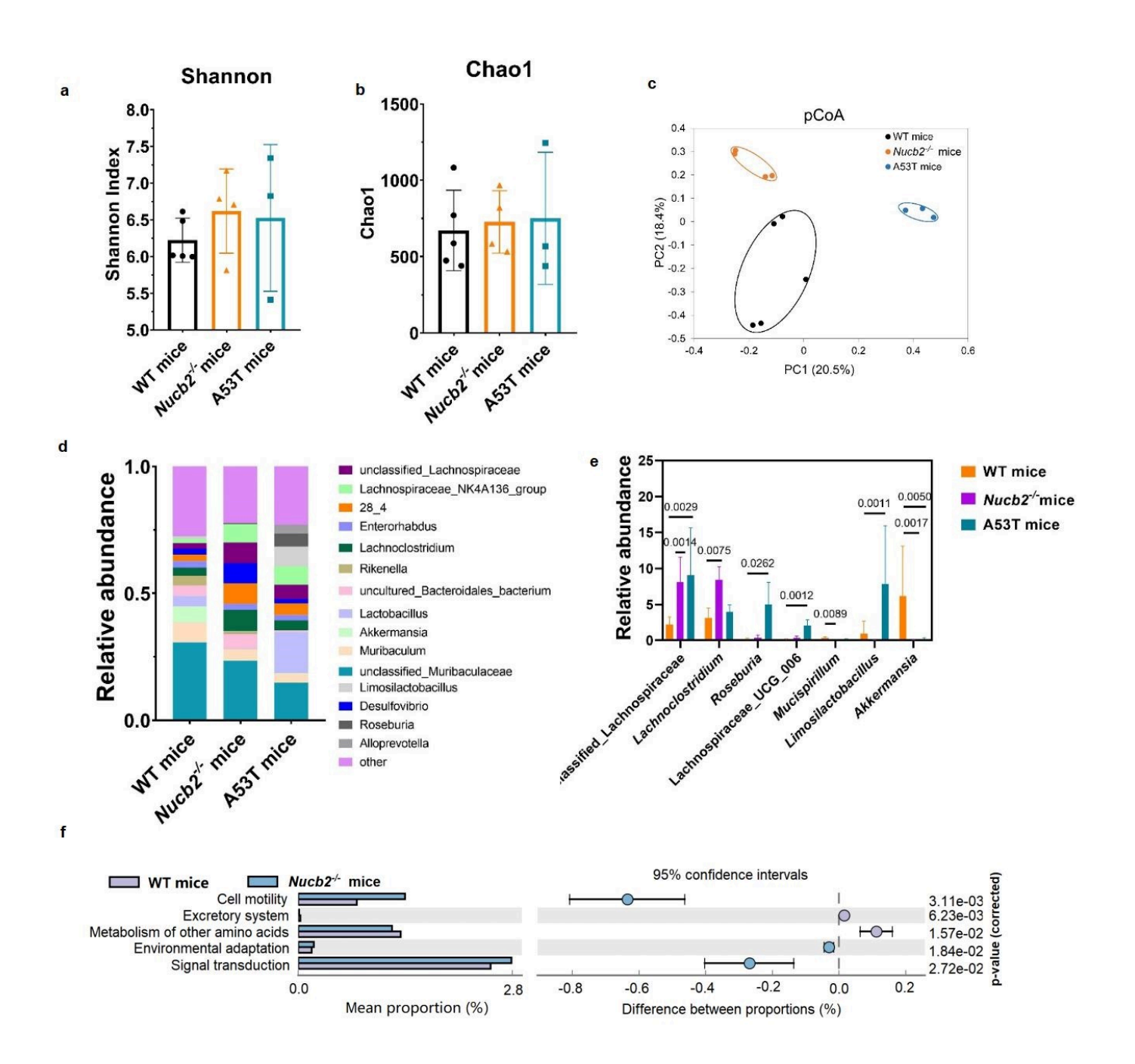


Figure 7

Analysis of intestinal bacterial community among different groups. **a** Shannon index of gut bacterial community in different groups. **b** Chao1 value of gut bacterial community in different groups. **c** Principal coordinates analysis (PCoA) of gut bacterial community. **d** Relative abundance of gut bacterial community at genus level. **e** Relative abundances of main genus with significant differences. **f** Differential analysis of KEGG metabolic pathways between groups. N = 3-5. **a**, **b**, Data were presented as mean ± SEM. 3m: 3-month-old, *Nucb2*: nucleobindin-2, *Nucb2*\(^-: Nucb2\) knockout, WT: wild-type.

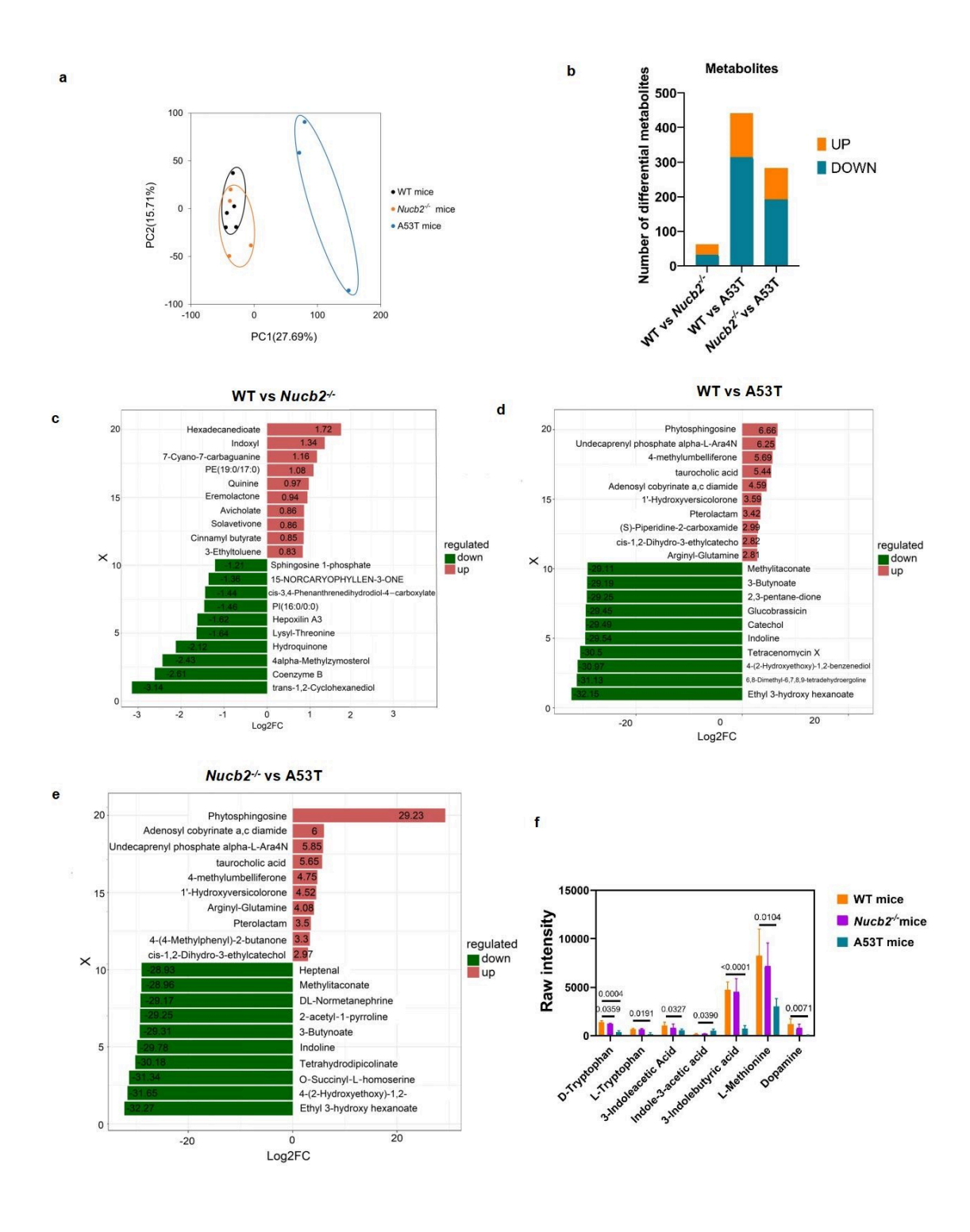


Figure 8

Metabolomic analysis of intestinal contents. a Principal Component Analysis (PCA) of different groups. **b** Number of differential metabolites between different groups. **c** Bar chart showing the fold differences in metabolites between WT and $Nucb2^{-/-}$ group. **d** Bar chart showing the fold differences in metabolites between WT and A53T group. **e** Bar chart showing the fold differences in metabolites between $Nucb2^{-/-}$ and A53T group. Only display the substances with the greatest difference in metabolic ratios (with 10 substances showing significant upregulation and 10 showing significant downregulation). **f** Histogram of main differential metabolites. n = 3. Nucb2: nucleobindin-2, $Nucb2^{-/-}$: Nucb2 knockout, WT: wild-type.

Supplementary Files

This is a list of supplementary files associated with this preprint. Click to download.

- nreditorialpolicychecklist.pdf
- nrreportingsummary.pdf